Korean J. Chem. Eng., 39(12), 3334-3342 (2022)
DOI: 10.1007/s11814-022-1128-x

pISSN: 0256-1115
eISSN: 1975-7220

Visible light photocatalytic activity of TiO_2 with carbon-fluorine heteroatoms simultaneously introduced by CF_4 plasma

Raneun Lee*, Chaehun Lim*, Hyeryeon Lee*, Seokjin Kim*, and Young-Seak Lee*,,†**

*Department of Chemical Engineering and Applied Chemistry, Chungnam National University, Daejeon 34134, Korea
**Institute of Carbon Fusion Technology (InCFT), Chungnam National University, Daejeon 34134, Korea
(*Received 11 February 2022 • Revised 18 March 2022 • Accepted 2 April 2022*)

Abstract−CF_4 plasma treatment is performed on commercial TiO_2 to improve the photocatalytic efficiency. The CF_4 plasma treatment is a facile and fast method for simultaneous introduction of carbon and fluorine atoms onto TiO_2. Photodegradation of rhodamine B, methyl orange, and methylene blue is carried out under solar light irradiation to determine its CF_4 plasma treatment effect. The dye removal of commercial TiO_2 to rhodamine B, methyl orange, and methylene blue is 60.0, 18.9, and 49.2%, respectively, whereas TiO_2 treated with CF_4 plasma for 50 min is 93.5, 71.0, and 88.6% for rhodamine B, methyl orange, and methylene blue, respectively. In addition, the photodegradation rate constants of TiO_2 treated with CF_4 plasma for 50 min were 0.0135, 0.0083, and 0.0129 min^{-1} for rhodamine B, methyl orange, and methylene blue, respectively, which are up to 7.5 times higher than that of untreated TiO_2 (0.0049, 0.0011, and 0.0039 min^{-1}). This improvement is attributed to the increase in oxygen vacancies by the introduction of carbon atoms into TiO_2 using CF_4 plasma treatment. In addition, the F^- ions physically adsorbed to the TiO_2 surface promote the formation of hydroxyl free radicals, enabling effective decomposition of various dyes.

Keywords: Titanium Dioxide, CF_4 Plasma, Photocatalytic Activity, Photocatalyst

INTRODUCTION

Recently, significant deterioration of the natural environment, including water and air, has been caused. Organic pollutants, which are extremely difficult to decompose by nature, can have serious adverse effects on water and air. Therefore, wastewater treatment is regarded as a major challenge worldwide [1-3]. Wastewater treatments include biological and chemical precipitation, membrane filtration, and ozone oxidation, but there are disadvantages, such as sludge generation, high treatment costs, and harsh temperature and treatment conditions [4]. In addition, existing treatment technologies have a common problem of generating secondary pollutants [5].

Among the methods used to remove water pollution, the photocatalyst is the most actively studied because it is environmentally friendly [5-7]. Photocatalysts promote photochemical reactions by using light as energy. Various photocatalysts, such as SiO_2, ZnO, WO_3, and TiO_2, have been used. Among them, TiO_2 is attracting a considerable amount of attention for use in environmental applications due to its strong light absorption, chemical stability, low cost, and high reactivity [1,4,5].

TiO_2, however, has a wide bandgap energy that makes decomposition of organic pollutants under solar light difficult [8]. Therefore, increasing the photocatalytic efficiency of TiO_2 even under visible light is an active area of research [9,10]. The use of dopants can improve the photocatalytic efficiency of TiO_2 because they narrow the bandgap. These dopants include light-absorbing substances (photosensitive agents, quantum dots, and dyes), transition metals, and nonmetal atoms. Metal doping, due to the high cost and high thermal instability of metals, has the disadvantage of an inferior photoactive effect, and so methods of doping with nonmetals have been widely studied [11-13].

In particular, fluorine plays a very important role in photocatalytic performance when introduced onto TiO_2 crystal surfaces. Kim et al. demonstrated that due to their high electronegativity, F^- ions that are physically adsorbed on the surface of TiO_2 inhibit the aggregation of TiO_2 particles and promote the formation of holes, thereby facilitating the decomposition of organic pollutants [14]. Therefore, the F^- species adsorbed on a TiO_2 surface play an important role in determining the photocatalytic efficiency. Carbon is also a common nonmetallic dopant that shows many advantages because of its excellent characteristics. Similar to metals, carbon possesses a large electron storage capacity that can accommodate photon-excited electrons, facilitating the separation of photogenic carriers [15-17].

Recently, codoped TiO_2 with nonmetals has become a rapidly growing field of interest. For example, Huang et al. prepared N-F codoped TiO_2 photocatalyst by a sol-gel solvothermal method. The doped N atoms improved the absorption of visible light, and the doped F atoms improved the surface acidity to increase the adsorption of the reactants, further enhancing the photocatalytic activity [18]. Therefore, there is the synergistic effect of N and F. Likewise, we conducted to improve the photocatalytic performance by doping carbon and fluorine on the TiO_2 surface through a very simple process. There are various methods of introducing carbon and fluorine atoms. The plasma method can introduce various atoms onto a TiO_2 surface by forming various ionic species using reactant such

†To whom correspondence should be addressed.
E-mail: youngslee@cnu.ac.kr

as SF_6, F_2, and CF_4. This process is facile, and depending on the reactant, various atoms can be doped [19,20].

Herein, we investigated the photodegradation of TiO_2 treated with CF_4 plasma. Through CF_4 plasma treatment, C and F atoms are simultaneously introduced onto TiO_2 to improve its photocatalytic performance. This increase in photocatalytic performance was measured by decomposition of various dyes under solar light.

EXPERIMENTAL

1. Materials and Reagents

Commercial TiO_2 (anatase, Sigma-Aldrich, USA) was used. The plasma reaction was carried out using high-purity tetrafluoromethane gas (99.99%, Deokyang Co., Korea) and nitrogen gas (99.999%, Special gas Co., Korea). In addition, 10 ppm rhodamine B (Acros organic, pure), 100 ppm methyl orange (Acros organic, pure), and 20 ppm methylene blue (Acros organic, pure) were prepared as the dye.

2. CF_4 Plasma Treatment

TiO_2 was prepared by plasma treatment using CF_4 gas at room temperature under vacuum. A plasma treatment system (CUTE; Femto-Science Co., Korea) consisting of an electrode, sample stage (size: 140×200 mm), gas inlet/outlet, mass flow controller, and vacuum system was used. TiO_2 (purchased from Sigma-Aldrich) was treated with CF_4 gas under vacuum plasma treatment conditions. The power (90 W), and CF_4 gas flow rate (80 sccm) were fixed and the reaction time was set to 10, 30, or 50 min; the samples were named $TiO_2/CF_4(10)$, $TiO_2/CF_4(30)$, and $TiO_2/CF_4(50)$, respectively.

3. Characterization of TiO_2-treated CF_4 Plasma

The surface morphology of various samples was observed using a field emission scanning electron microscope (FE-SEM, S-4800, Hitachi, Japan, with 15 kV of accelerating voltage) with energy dispersive X-ray spectroscopy (EDS, Oxford X-Max 50, Oxford, UK). The surface chemical properties were determined by X-ray photoelectron spectroscopy (XPS, AXIS SUPRA, Kratos, UK) with a monochromatic Al Kα source (1,486.6 eV), and the binding energy was referenced to the C1s peaks at 284.5 eV corresponding to surface adventitious carbon. The crystallographic structure of various samples was determined using X-ray diffraction (XRD, Malvern PANalytical X'pert pro equipped with Cu Kα radiation, England). In addition, the photocatalytic property of TiO_2-treated CF_4 plasma was measured by ultraviolet-visible-infrared spectrophotometer (UV-VIS-IR, Cary 5G, Agilent, USA) and high-resolution photoluminescence spectroscopy (PL, a LabRAM HR-800 spectrometer, Horiba, Japan).

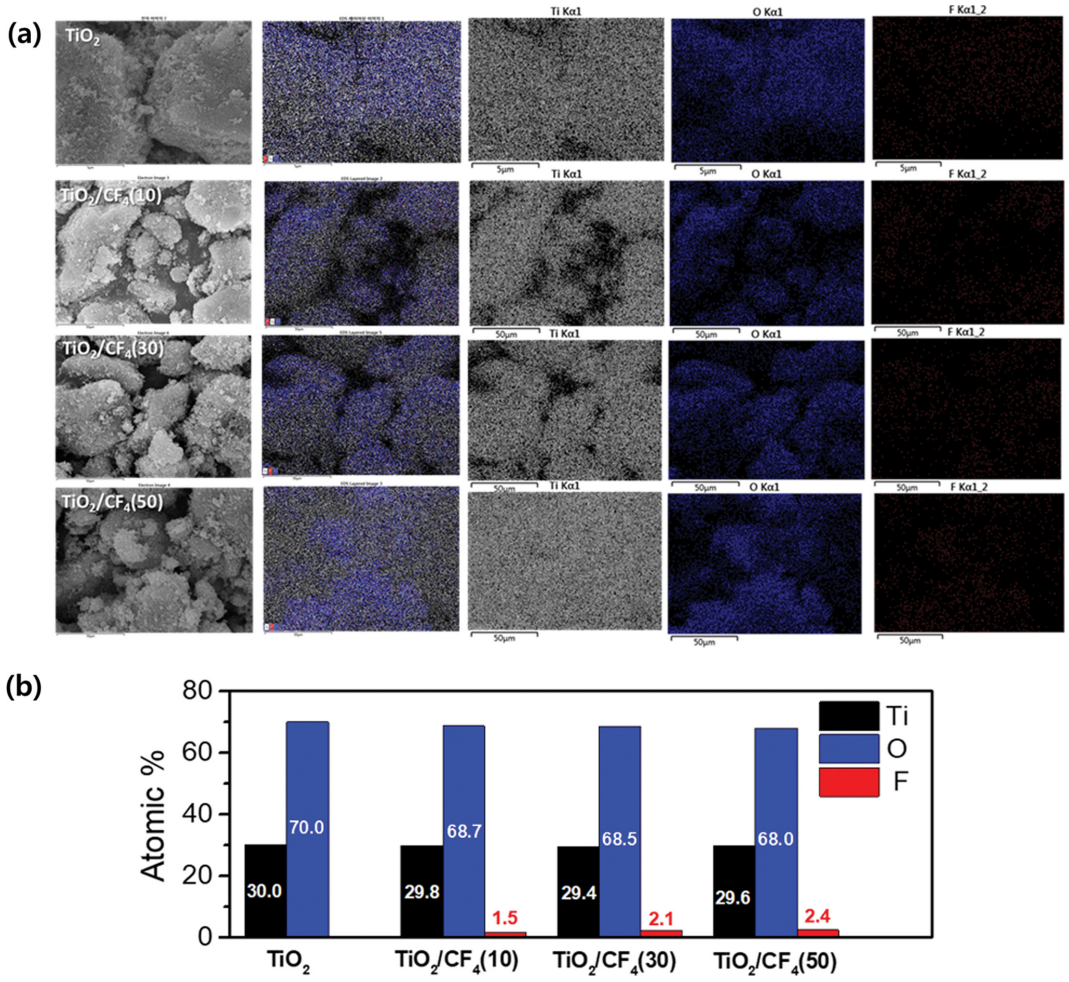

Fig. 1. (a) SEM-EDS images and (b) atomic percentages of pristine TiO_2, $TiO_2/CF_4(10)$, $TiO_2/CF_4(30)$, and $TiO_2/CF_4(50)$.

4. Photocatalytic Activity

The photocatalytic activity of each sample was evaluated by photodegradation of rhodamine B (RhB, ACROS organics), methyl orange (MO, ACROS organics), and methylene blue (MB, ACROS organics) under a solar simulator (PEC-L01, Peccell Technologies, Japan) with a 150 W Xe lamp. The CF_4-treated TiO_2 powders (50 mg) were dispersed in 100 mL of 10 ppm RhB, 100 ppm MO, and 20 ppm MB. The dye solution was extracted at certain intervals during irradiation with artificial solar light, and the concentration of the dye was determined via a UV-visible spectrophotometer (UV-Vis, Optizen 2120UV, Mecasys, Korea). The concentration was calculated by the Beer-Lambert law. The equation is below.

$$A=\varepsilon bc \quad (1)$$

A is the absorbance, ε is the adair molar attenuation coefficient or absorptivity of the attenuating species, b is the optical path length in cm, and c is the concentration of the attenuating species. The photocatalytic decomposition data was measured repeatedly three times, and then averaged to show the standard deviation.

RESULTS AND DISSCUSION

1. The Surface Properties of the Samples

Fig. 1 shows the SEM-EDS images of the samples. Fig. 1(a) shows pristine TiO_2, and Fig. 1(b)-(d) shows CF_4 plasma-treated TiO_2. In comparison, the samples shown in Fig. 1(b), (c), and (d) are less agglomerated than pristine TiO_2 (Fig. 1(a)). These results show the inhibition of particle aggregation induced by the CF_4 plasma. Aggregation influences the optical property and photocatalytic activity of materials because the number of sites where organic compounds

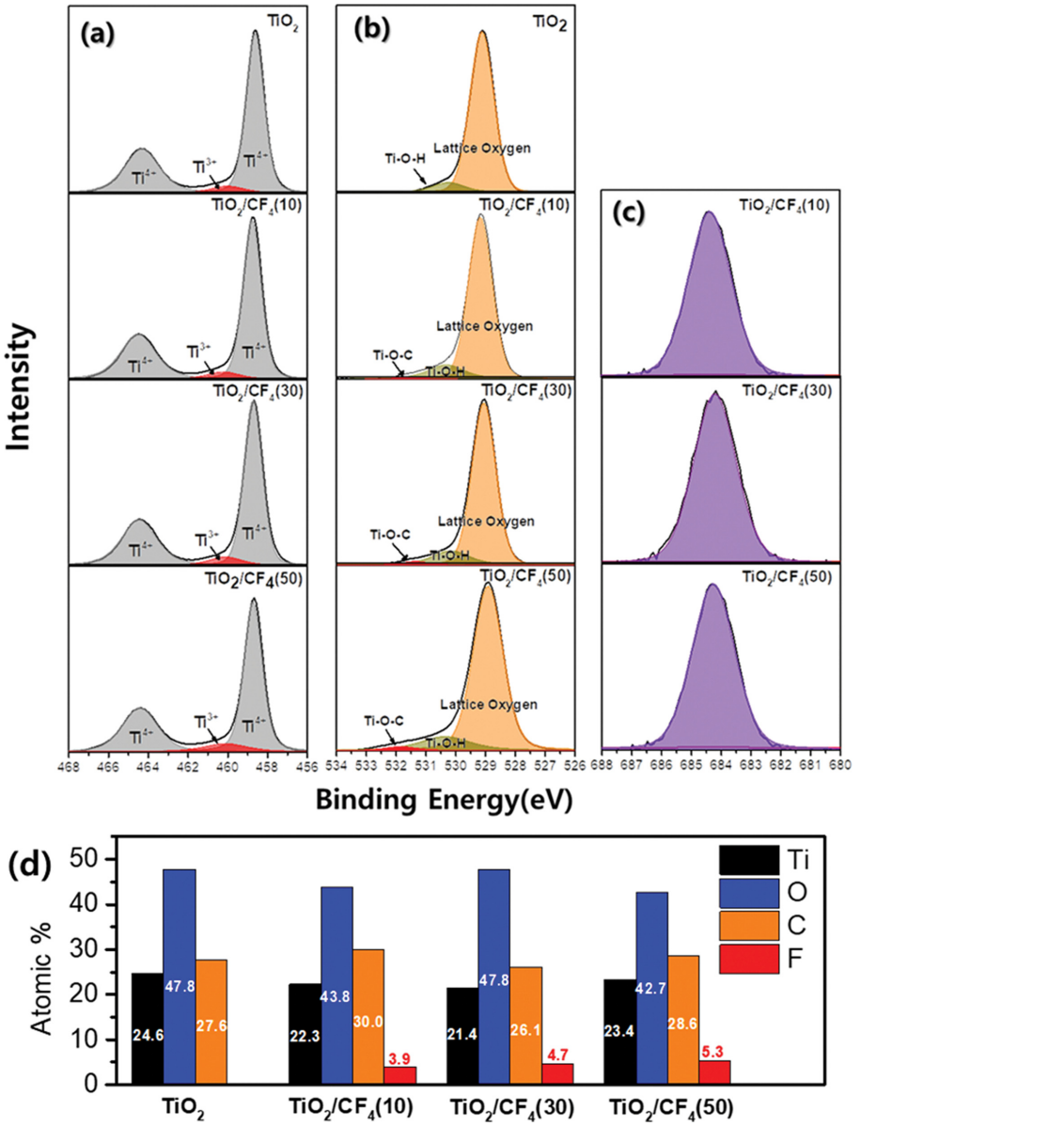

Fig. 2. XPS (a) Ti_{2p}, (b) O1s, and (c) F1s core level deconvolution spectra of TiO_2 and CF_4 treated TiO_2 and (d) atomic percentage of TiO_2 and CF_4 treated TiO_2.

Table 1. The area of each peak in the XPS spectra converted to a percentage (a) O1s and (b) Ti_{2p}

(a) Ti_{2p} peak parameter

	TiO_2	$TiO_2/CF_4(10)$	$TiO_2/CF_4(30)$	$TiO_2/CF_4(50)$
Ti^{4+}	59.8	59.0	58.6	58.6
Ti^{3+}	5.3	5.5	6.3	7.9
Ti^{4+}	34.9	35.5	35.1	33.5

(b) O1s peak parameter

	TiO_2	$TiO_2/CF_4(10)$	$TiO_2/CF_4(30)$	$TiO_2/CF_4(50)$
Lattice oxygen	91.1	89.0	85.6	84.5
Ti-O-H	8.9	10.4	12.9	13.6
Ti-O-C	-	0.6	1.5	1.9

are decomposed increases [21-23]. In addition, the EDS image shows fluorine doping on the TiO_2 surface. F element content of pristine TiO_2, $TiO_2/CF_4(10)$, $TiO_2/CF_4(30)$, $TiO_2/CF_4(50)$ is 0.0, 1.5, 2.1 and 2.4 at%, respectively. As the plasma reaction time increases, the F content also increases. However, as the reaction time increases, the difference in fluorine content between samples decreases because the amount of fluorine introduced to the TiO_2 surface is limited [24].

Fig. 2(a) shows the high resolution XPS spectra of the Ti_{2p} region of untreated and CF_4 treated TiO_2. The peaks located at 458.8, 460.3, and 464.5 eV correspond to those of $Ti^{4+}(2p_{3/2})$, $Ti^{3+}(2p_{1/2})$, and $Ti^{4+}(2p_{1/2})$, respectively [18,23-27]. Table 1(a) shows the values converted to percentages by calculating the area of each peak in the Ti_{2p} graph. As the plasma reaction time increases, the Ti^{3+} peak area increases by up to 2.6%. The change in the oxidation state from Ti^{4+} to Ti^{3+} corresponds to an increase in the number of oxygen vacancies [3,26]. The results in Table 1 indicate that as CF_4 plasma treatment is performed on TiO_2, the number of oxygen vacancies increases, and the photocatalytic activity increases [26,28].

Fig. 2(b) shows the O1s spectra of pristine and CF_4 plasma treated TiO_2, with peaks at 530.0 and 531.5 eV. The peak of the lower binding energy is assigned to the bulk oxygen atoms in the TiO_2 lattice forming Ti-O-Ti groups, and the peak of the higher binding energy indicates hydroxyl groups in the form of Ti-O-H on the TiO_2 surface. In addition, as the generation time increases, a Ti-O-C peak forms near 532.6 eV because the plasma treatment creates CF_4 active species, such as ·CF_3, ·CF_2, ·CF, and ·F [19,29]. The C atoms from CF_4 active species are thought to substitute for TiO_2. The longer the reaction time is, the more plasma energy is received on the TiO_2 surface, so more carbon atoms are substituted. Therefore, Ti-O-C bonding decreases the amount of lattice oxygen, which can increase the number of oxygen vacancies, leading to improvement of photocatalysis of CF_4 treated TiO_2 [30,31]. Table 1(b) shows the values obtained by integrating each peak in the O1s graph and expressing the results as percentages. The percentage of the lattice oxygen peak near 530.0 eV decreases by up to 6.6% as the plasma reaction time increases. This means that the number of oxygen vacancies increases as the plasma reaction time increases. It has been reported that surface oxygen vacancies not only react strongly to visible light, but also act as traps to inhibit electron-hole recombination [30,31].

The XPS spectra of untreated and CF_4 plasma-treated TiO_2 are presented in Fig. 2. In the spectra of the CF_4-treated TiO_2 samples shown in Fig. 2(c), the F 1s peak was observed at the binding energy of 684.5 eV. This indicates that F^- is physically adsorbed on the TiO_2 surface. Generally, there are the peaks near 688.1 eV which correspond to F^- ions substituted for O within the TiO_2 crystal lattice. This peak cannot be seen in Fig. 2(c), indicating that F^- ions were not doped in the crystal lattice of TiO_2 [21,22]. F^- ions that are physically adsorbed onto TiO_2 surface play an important role in preventing particle aggregation [14,23,25]. Because of the high electronegativity of F, the surface of F^- adsorbed TiO_2 becomes negatively charged, and the repulsive force between the particles increases, thereby inhibiting aggregation [14]. This conclusion is consistent with the SEM results.

2. XRD Analysis and UV-vis Adsorption Measurements of the Samples

TiO_2, as a photocatalyst, has three crystalline forms: anatase, brookite, and rutile. As shown in Fig. 3, pristine and CF_4 plasma treated TiO_2 are well crystallized as pure-phase anatase TiO_2. The typical diffraction peaks of anatase TiO_2 at 2θ=25.29°, 37.09°, 37.96°, 38.46°, 48.25°, 53.93°, 55.06°, 62.67°, 68.90°, 70.45°, and 75.15° can be indexed to (101), (103), (004), (112), (200), (105), (211), (204),

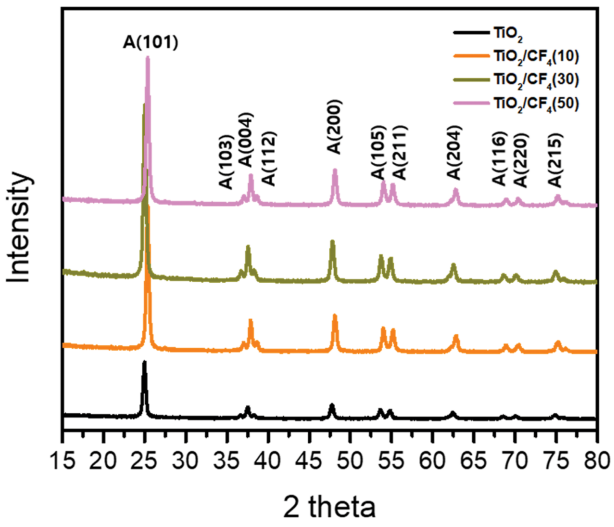

Fig. 3. XRD patterns of TiO_2, $TiO_2/CF_4(10)$, $TiO_2/CF_4(30)$, and $TiO_2/CF_4(50)$.

(116), (220), and (215), respectively [23,33,34]. The samples are not shown as rutile or brookite crystal structure due to the low applied plasma energy. Since the active species formed by the CF_4 plasma were not introduced into the TiO_2 crystal lattice, the crystallinity

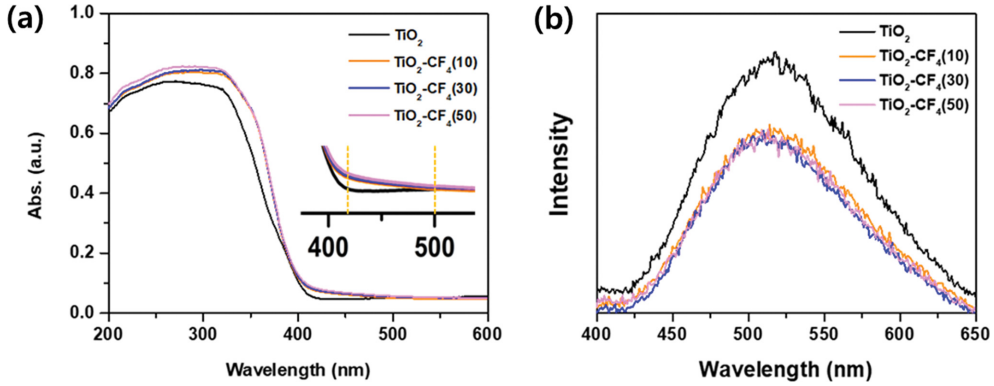

Fig. 4. (a) UV-vis adsorption spectra and (b) PL analysis of TiO_2, $TiO_2/CF_4(10)$, $TiO_2/CF_4(30)$, and $TiO_2/CF_4(50)$ between 200 and 600 nm.

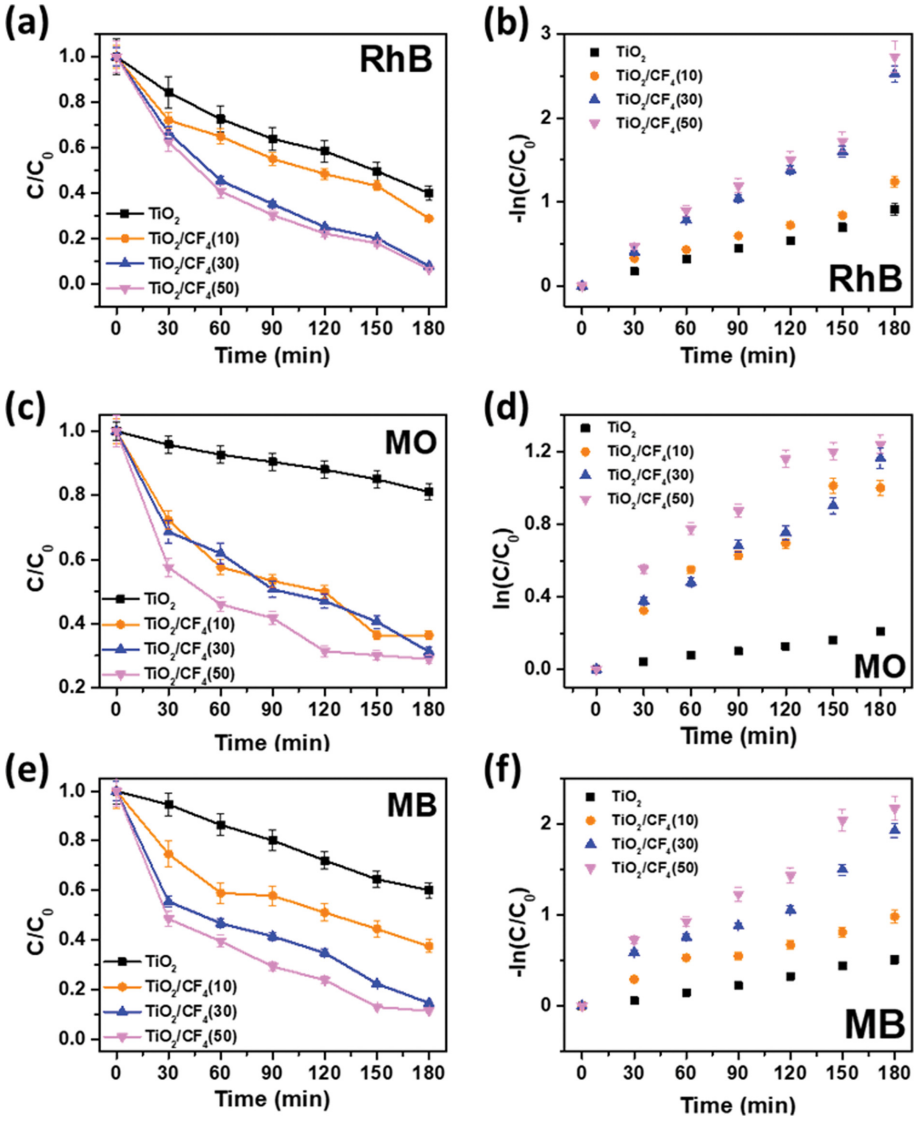

Fig. 5. Photocatalytic degradation of rhodamine B (a)-(b), methyl orange (c)-(d), and methylene blue (e)-(f) with TiO_2, $TiO_2/CF_4(10)$, $TiO_2/CF_4(30)$, and $TiO_2/CF_4(50)$ under solar light.

did not change, but the intensity of each peak increased, indicating that the plasma treatment favors crystallization [23]. In general, the anatase type of TiO_2 has been reported to have the best photocatalytic performance [33-35]. Therefore, each peak of anatase increased due to the CF_4 plasma treatment, which also affected photocatalytic performance.

The UV-vis absorption spectra of pristine and CF_4 plasma-treated TiO_2 are shown in Fig. 4(a). CF_4 plasma-treated TiO_2, shows higher light adsorption above 420 nm than pristine TiO_2 which exhibit redshift in the band gap transition, in good agreement with the activity of the photocatalyst [33]. These results indicate that CF_4 plasma treatment can shift the adsorption edge of TiO_2 to the visible region. As shown in Fig. 2, CF_4-treated TiO_2 has more oxygen vacancies, shifting the adsorption to approximately 500 nm. Moreover, the adsorption peaks of CF_4 plasma-treated TiO_2 below 400 nm are stronger than those of pristine TiO_2. This has an effect on the photocatalytic activity of TiO_2 under solar light containing 5% UV light [36].

PL spectra of pristine and CF_4 plasma-treated TiO_2 were measured to study the separation efficiency of photogenerated electrons and holes at room temperature. Fig. 4(b) exhibits the PL spectra of all samples excited at 316 nm. The CF_4-treated TiO_2 show lower PL intensity than pristine TiO_2 because photogenerated charge can migrate to the carbon or fluorine region. Generally, the decrease of PL intensity indicates the efficient electron-hole separation and long-lived carriers [37-39].

3. Photocatalytic Activity of Samples

To evaluate the photocatalyst performance of CF_4 plasma-treated TiO_2, rhodamine B dye was decomposed under solar light. Based on the Beer-Lambert equation, Fig. 5(a)-(b) shows the degradation of rhodamine B under solar light irradiation to compare the photocatalytic performance between of pristine TiO_2 and TiO_2-treated CF_4 plasma. As shown in Fig. 5(b), the degradation of rhodamine B containing TiO_2 obeys pseudo-first-order kinetics, following the equation below [28,39]:

$$-\ln[C/C_0]=kt \quad (2)$$

where C_0 is the initial concentration of dye and C is the concentration at time. The dye removal of TiO_2 is 60.0%, whereas the dye removal properties of $TiO_2/CF_4(10)$, $TiO_2/CF_4(30)$, and $TiO_2/CF_4(50)$ are 71.1, 92.0, and 93.5%, respectively. Table 2 shows the values of the correlation coefficient (R^2) and rate constant (k) calculated by the pseudo-first-order kinetics equation. Fig. 5(b) and Table 2 indicate that the photodegradation rates constant, k, related to the degradation efficiency was 0.0049 min^{-1} for pristine TiO_2, 0.0064 min^{-1} for $TiO_2/CF_4(10)$, 0.0124 min^{-1} for $TiO_2/CF_4(30)$, and 0.0135 min^{-1} for $TiO_2/CF_4(50)$. After 180 min of solar light irradiation, TiO_2 treated CF_4 plasma exhibited greater degradation efficiency than pristine TiO_2, removing up to 93.5% of rhodamine B, and the photodegradation rate constant (k) increased up to 2.1 times.

Fig. 5(c)-(d) shows the methyl orange (MO) degradation of pristine TiO_2 and CF_4 plasma treated TiO_2. As shown in Fig. 5(c), the dye removal of TiO_2 is 18.9%, whereas the dye removal properties of $TiO_2/CF_4(10)$, $TiO_2/CF_4(30)$, and $TiO_2/CF_4(50)$ are 63.6, 68.8, and 71.0%, respectively. In addition, Fig. 5(d) and Table 2 show the MO photodegradation rates constant constant (k) of pristine TiO_2 and TiO_2 treated with CF_4 plasma. photodegradation rates constant (k) of pristine TiO_2, $TiO_2/CF_4(10)$, $TiO_2/CF_4(30)$, and $TiO_2/CF_4(50)$ are 0.0011, 0.0063, 0.0066, and 0.0083 min^{-1}. Both the dye removal and photodegradation rates constant (k) of TiO_2 treated with CF_4 increased despite the very high concentration of MO as 100 ppm.

Fig. 5(d)-(e) shows the methylene blue (MB) degradation of pristine TiO_2 and CF_4 plasma treated TiO_2. The dye removal of TiO_2, $TiO_2/CF_4(10)$, $TiO_2/CF_4(30)$, and $TiO_2/CF_4(50)$ are 49.2, 62.6, 85.5 and 88.6%, respectively. Moreover, as shown in Fig. 5(e) and Table 2, the photodegradation rate constant (k) of pristine TiO_2, $TiO_2/CF_4(10)$, $TiO_2/CF_4(30)$, and $TiO_2/CF_4(50)$ is 0.0039, 0.0057, 0.0103, and 0.0129 min^{-1}, respectively. The MB dye removal property of TiO_2 treated with CF_4 plasma was increased up to 80.1%, and the photodegradation rate constant (k) was increased up to 3.3 times. In terms of photocatalytic performance, $TiO_2/CF_4(50)$ is the best, but the difference decreases gradually when compared to $TiO_2/CF_4(10)$ and $TiO_2/CF_4(30)$. This is because the functional group impregnation is limited over time.

According to the XPS results (Fig. 2), the peak of F^- adsorbed on TiO_2 is shown in the F1s spectrum. Such ions physically adsorbed on the TiO_2 surface can decompose organic compounds by the following mechanism [18,32]:

$$\equiv Ti\text{-}OH+F^- \rightarrow \equiv Ti\text{-}F+OH^- \quad (3)$$

$$\equiv Ti\text{-}F+h^++H_2O \rightarrow \equiv Ti\text{-}F+\bullet OH_{free}+H^+ \quad (4)$$

≡Ti-F bonds are formed by surface modification of hydroxyl groups on the TiO_2 surface (Eq. (3)). The surface ≡Ti-F bonds have a strong electron-trapping ability and can decrease the rate of recombination of electron-hole pairs [25,40,41]. Moreover, F^- adsorbed on TiO_2 creates a large number of holes, increasing the yield of hydroxyl radicals. The proposed mechanism is shown in Fig. 6. The formation of free OH radicals on the CF_4 plasma-treated TiO_2 surface is

Table 2. Photodegradation rate constant (k) of various dye calculated by the pseudo-first order rate equation and its correlation coefficient (R^2)

Sample	Rhodamine B		Methyl orange		Methylene blue	
	k	R^2	k	R^2	k	R^2
TiO_2	0.0049	0.9890	0.0011	0.9900	0.0039	0.9600
$TiO_2/CF_4(10)$	0.0064	0.9520	0.0063	0.9042	0.0057	0.9141
$TiO_2/CF_4(30)$	0.0124	0.9582	0.0066	0.9348	0.0103	0.9399
$TiO_2/CF_4(50)$	0.0135	0.9558	0.0083	0.8637	0.0129	0.9451

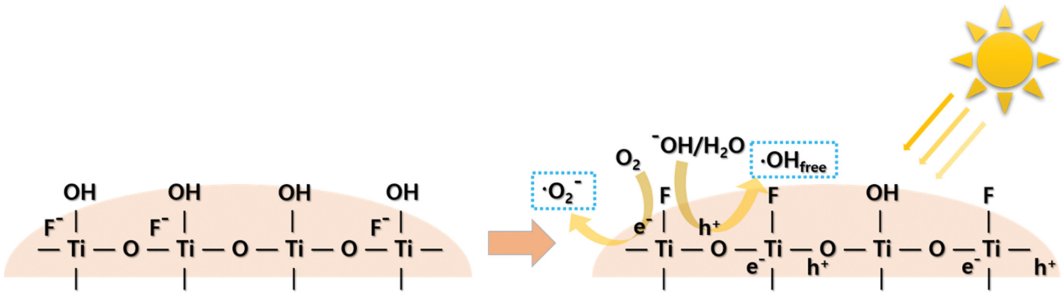

Fig. 6. Proposed mechanism to form OH free radicals from F^- adsorbed on the surface of TiO_2. The left panel shows TiO_2 treated CF_4 plasma, and the right panel shows the reaction of TiO_2 treated CF_4 plasma occurring in dye solution under solar light.

Table 3. Rhodamine B degradation performance of CF_4 plasma treated TiO_2 compared with other literature

Material	Light source	Dye	Amount of catalyst (mg)	Concentration of dye (ppm)	Degradation rate (%)	Exposed time (min)	Ref.
TiO_2-CF_4 (50)	Solar simulator	Rhodamine B	50	10	93.5	180	This study
TiO_2-CF_4 (50)	Solar simulator	Methly orange	50	100	71.0	180	This study
TiO_2-CF_4 (50)	Solar simulator	Methylene blue	50	20	88.6	180	This study
$BiVO_4$/TiO_2	Visible	Rhodamine B	80	1	79	360	[50]
F-doped TiO_2	Xenon lamp	Rhodamine B	100	10	Approximately 95	360	[51]
N-doped TiO_2/ZnO	254 nm UV lamp	Methyl orange	100	25	Approximately 70	180	[52]
Polyamide-C/TiO_2	Visible light	Methylene blue	100	5	82.7	300	[53]

expected to subsequently oxidize the organic compound [25,35, 41-43].

As shown in Fig. 2 and Table 1, the number of oxygen vacancies increases upon CF_4 plasma treatment because of C atom doping. The creation of Ti-O-C bonds can create oxygen vacancies. The oxygen vacancies play an important role in enhanced photodegradation [30,31,44]. In addition, carbon is well known as a material with easy electron movement. As reported by Lettmann et al., it plays a role in smoothing the movement of electrons in the bandgap when C is doped TiO_2 [45,46]. Therefore, the number of oxygen vacancies and OH free radicals increased due to the synergistic effect of carbon and fluorine atoms introduced into TiO_2. This led to an improved photocatalytic performance.

The results of photodegradation for the three dyes vary depending on the surface charge of the dye molecules, their interaction with the photocatalyst, the chemistry, and binding of the dyes. In general, Rh B and MB are cationic dyes, and MO is anionic dye [47]. MB has superior photodegradation at high concentration compared to Rh B. Although both are cationic dyes, MB strongly adsorbs to the CF_4 plasma-treated TiO_2 surface compared to Rh B. This is because MB has a relatively small molecular size compared to Rh B, which indicates a steric hindrance [48]. Compared to Rh B and MB, MO was able to decompose even at a high concentration of 100 ppm. This is because MO molecules are oxidized by OH free radicals formed by the CF_4 plasma [49].

Moreover, the Rh B, MO, and MB photodegradation of CF_4-treated TiO_2 was compared to that of the TiO_2 photocatalyst in another reference, as shown in Table 3. Although different conditions were used, the catalysts used in this study performed better. The authors of Hu performed rhodamine B dye decomposition by doping metal into TiO_2 [50]. However, compared to the conditions used in this experiment, the time of exposure to light energy was longer but the dye removal property was increased, so the photocatalytic performance of CF_4-treated TiO_2 was better. This shows that the effect is better in the case of nonmetal doping than in the case of metal doping. In addition, a difference in rhodamine B decomposition performance was observed even in F-doped TiO_2. According to Li et al., the dye decomposition efficiency of F-doped TiO_2 was almost 95% after light irradiation for six hours, and the amount of catalyst was approximately twice that of used in this study. At 180 min, the rhodamine B dye removal property was approximately 93.5% [51]. Moreover, Tian reported MO removal of N doped TiO_2/ZnO composites. Although the concentration of MO was 25 ppm, the dye removal property was only about 70% decomposed in three hours [52]. On the other hand, in this study, despite the use of a high concentration of 100 ppm MO, its dye removal property of CF_4 treated TiO_2 was 71.0% in three hours. Amran et al. performed MB removal using polyamide-C/TiO_2. When the catalyst amount was 100 mg and the MB concentration was 5 ppm, the degradation rate of MB for 300 minutes under visible light was 82.7%. In this study, when 20 ppm of MB was decomposed for 180 min with 50 mg of catalyst, the dye removal property was 88.6% [53]. This is attributed to multiple doping of C and F.

CONCLUSION

TiO_2 powder was modified by CF_4 plasma at room temperature with different reaction time to improve its photocatalytic activity. The dye removal properties of rhodamine B, methyl orange, and methylene blue of commercial TiO_2 were 60.0, 18.9, and 49.2%,

respectively, whereas TiO_2/CF_4(50) was 93.5, 71.0, and 88.6%, respectively. The introduction of C and F atoms on the TiO_2 surface by CF_4 plasma increased the number of oxygen vacancies, and the F^- ions on the surface promoted the formation of OH radicals, thereby increasing the photocatalytic efficiency. However, the increase in the decomposition efficiency of rhodamine B decreased as the reaction time increased, which is believed to be due to the limited number of functional groups introduced onto the TiO_2 surface. In conclusion, CF_4 plasma treatment is a facile method to improve photocatalytic activity by enabling the simultaneous introduction of C atoms and F atoms onto the TiO_2 surface.

ACKNOWLEDGEMENT

This work was supported by Industrial Strategic Technology Development Program (20012763, Development of petroleum residue-based porous adsorbent for industrial wastewater treatment) funded by the Ministry of Trade, Industry & Energy (MOTIE, Korea).

REFERENCES

1. D. Chen, Y. Cheng, N. Zhou, P. Chen, Y. Wang, K. Li, S. Huo, P. Cheng, P. Peng and R. Zhang, *J. Clean. Prod.*, **268**, 121725 (2020).
2. S. MiarAlipour, D. Friedmann, J. Scott and R. Amal, *J. Hazard. Mater.*, **341**, 404 (2018).
3. H.-R. An, S. Y. Park, J. Y. Huh, H. Kim, Y.-C. Lee, Y. B. Lee, Y. C. Hong and H. U. Lee, *Appl. Catal. B.*, **211**, 126 (2017).
4. Y. Ling, J. Li, J. Wu, H. Liu, X. Mao, Y. Qi, Q. Ma, Q. Liu, Z. Qiao and W. Chu, *J. Chem. Eng.*, **39**, 343 (2022).
5. T. S. Kazeem, M. Zubair, M. Daud, N. D. Mu'azu and M. A. Al-Harthi, *J. Chem. Eng.*, **36**, 1057 (2019).
6. K. Hossienzadeh, A. Maleki, H. Daraei, M. Safari, R. Pawar and S. M. Lee, *J. Chem. Eng.*, **36**, 1360 (2019).
7. A. Sridhar, M. Ponnuchamy, A. Kapoor and S. Prabhakar, *J. Hazard. Mater.*, **424**, 127432 (2022).
8. D. H. Kang, H. Jo, M.-J. Jung, K. H. Kim and Y.-S. Lee, *Carbon Lett.*, **27**, 64 (2018).
9. J. S. Lee, K. H. You and C. B. Park, *Adv. Mater.*, **24**, 1084 (2012).
10. M. Baruah, S. L. Ezung, A. Supong, P. C. Bhomick, S. Kumar and D. Sinha, *J. Chem. Eng.*, **38**, 1277 (2021).
11. M. Zafar, J.-Y. Yun and D.-H. Kim, *J. Chem. Eng.*, **35**, 567 (2018).
12. J.-Y. Jung, J. H. Kim and Y.-S. Lee, *J. Nanosci. Nanotechnol.*, **16**, 4498 (2016).
13. M.-J. Jung, Y. Kim and Y.-S. Lee, *J. Ind. Eng. Chem.*, **47**, 187 (2017).
14. J.-H. Kim, F. Nishimura, S. Yonezawa and M. Takashima, *J. Fluor. Chem.*, **144**, 165 (2012).
15. F. Teng, G. Zhang, Y. Wang, C. Gao, L. Chen, P. Zhang, Z. Zhang and E. Xie, *Appl. Surf. Sci.*, **320**, 703 (2014).
16. G.-w. Cui, W.-l. Wang, M.-y. Ma, M. Zhang, X.-y. Xia, F.-y. Han, X.-f. Shi, Y.-q. Zhao, Y.-B. Dong and B. Tang, *Chem. Comm.*, **49**, 6415 (2013).
17. Y.-T. Lin, C.-H. Weng, Y.-H. Lin, C.-C. Shiesh and F.-Y. Chen, *Sep. Purif. Technol.*, **116**, 114 (2013).
18. D.-G. Huang, S.-J. Liao, J.-M. Liu, Z. Dang and L. Petrik, *J. Photochem. Photobiol. A: Chem.*, **184**, 282 (2006).
19. R. Lee, C. Lim, M.-J. Kim and Y.-S. Lee, *Appl. Chem. Eng.*, **32**, 55 (2021).
20. E. J. Song, M.-J. Kim, J.-I. Han, Y. J. Choi and Y.-S. Lee, *Appl. Chem. Eng.*, **30**, 160 (2019).
21. Y. Park, W. Kim, D. n. Monllor-Satoca, T. Tachikawa, T. Majima and W. Choi, *J. Phys. Chem. Lett.*, **4**, 189 (2013).
22. F. Pellegrino, L. Pellutiè, F. Sordello, C. Minero, E. Ortel, V.-D. Hodoroaba and V. Maurino, *Appl. Catal. B*, **216**, 80 (2017).
23. Y. He, Q. Yan, X. Liu, M. Dong and J. Yang, *J. Photoch. Photobio. A*, **393**, 112400 (2020).
24. M. H. Lee, H. Y. Kim, J. Kim, J. T. Han, Y.-S. Lee and J. S. Woo, *Carbon Lett.*, **30**, 345 (2020).
25. D.-H. Lee, B. Swain, D. Shin, N.-K. Ahn, J.-R. Park and K.-S. Park, *Mater. Res. Bull.*, **109**, 227 (2019).
26. B. Bharti, S. Kumar, H.-N. Lee and R. Kumar, *Sci. Rep.*, **6**, 1 (2016).
27. N. Mahdi, P. Kumar, A. Goswami, B. Perdicakis, K. Shankar and M. Sadrzadeh, *Nanomaterials*, **9**, 1186 (2019).
28. S. Kaur and V. Singh, *J. Hazard. Mater.*, **141**, 230 (2007).
29. Y. Zhang, Z. Chen and Z. Lu, *Nanomaterials*, **8**, 261 (2018).
30. T. R. Gordon, M. Cargnello, T. Paik, F. Mangolini, R. T. Weber, P. Fornasiero and C. B. Murray, *J. Am. Chem. Soc.*, **134**, 6751 (2012).
31. J. Li, M. Zhang, Z. Guan, Q. Li, C. He and J. Yang, *Appl. Catal. B*, **206**, 300 (2017).
32. Y. He, Q. Yan, X. Liu, M. Dong and J. Yang, *J. Photoch. Photobio. A*, **393**, 112400 (2020).
33. H.-Y. Kim and Y.-W. Ju, *J. Chem. Eng.*, **38**, 1522 (2021).
34. B. Bharti, H. Li, D. Liu, H. Kumar, V. Manikandan, X. Zha and F. Ouyang, *Appl. Phys. A*, **126**, 1 (2020).
35. Y. Sang, H. Liu and A. Umar, *Chem. Pub. Soc. Europe.*, **7**, 559 (2015).
36. S.-y. Yang, Y.-y. Chen, J.-g. Zheng and Y.-j. Cui, *J. Environ. Sci.*, **19**, 86 (2007).
37. N. Yao, J. Huang, K. Fu, X. Deng, M. Ding, S. Zhang, X. Xu and L. Li, *Sci. Rep.*, **6**, 31123 (2016).
38. Y. Chen, Y. Wang, W. Li, Q. Yang, Q. Hou, L. Wei, L. Liu, F. Huang and M. Ju, *Appl. Catal. B*, **210**, 352 (2017).
39. H. U. Lee, Y.-C. Lee, S. C. Lee, S. Y. Park, B. Son, J. W. Lee, C.-H. Lim, C.-J. Choi, M.-H. Choi and S. Y. Lee, *Chem. Eng. J.*, **254**, 268 (2014).
40. C. Minero, G. Mariella, V. Maurino and E. Pelizzetti, *Langmuir*, **16**, 2632 (2000).
41. K. Lv, B. Cheng, J. Yu and G. Liu, *Phys. Chem.*, **14**, 5349 (2012).
42. J. Liu, F. Xie, R. Li, T. Li, Z. Jia, Y. Wang, Y. Wang, X. Zhang and C. Fan, *Mater. Sci. Semicond. Process.*, **97**, 1 (2019).
43. Q. Liu, F. Wang, H. Lin, Y. Xie, N. Tong, J. Lin, X. Zhang, Z. Zhang and X. Wang, *Catal. Sci. Technol.*, **8**, 4399 (2018).
44. Y. Zhang, Z. Chen and Z. Lu, *Nanomaterials*, **8**, 261 (2018).
45. C. Lettmann, K. Hildenbrand, H. Kisch, W. Macyk and W. F. Maier, *Appl. Catal. B*, **32**, 215 (2001).
46. B. C. Bai, J. S. Im, J. G. Kim and Y.-S. Lee, *Appl. Chem. Eng.*, **21**, 29 (2010).
47. H. W. Jeon, M. G. Jeong, B. Y. An, M. S. Hong, S. H. Seong and G. D. Lee, *Clean Technol.*, **26**, 311 (2020)
48. D. Zhang, J. Li, Q. Wang and Q. Wu, *J. Mater. Chem. A*, **1**, 8622 (2013).
49. F. Huang, L. Chen, H. Wang, T. Feng and Z. Yan, *J. Electrostat.*, **70**, 43 (2012).

50. C. Li, Z. Sun, R. Ma, Y. Xue and S. Zheng, *Micropor. Mesopor. Mater.*, **243**, 281 (2017).
51. J. Tian, J. Wang, J. Dai, X. Wang and Y. Yin, *Surf. Coat. Technol.*, **204**, 723 (2009).
52. S. N. B. S. Amran, V. Wongso, N. S. A. Halim, M. K. Husni, N. S. Sambudi and M. D. H. Wirzal, *J. Asian Ceram. Soc.*, **7**, 321 (2019).
53. D.-G. Huang, S.-J. Liao, J.-M. Liu, Z. Dang and L. Petrik, *J. Photochem. Photobiol. A*, **184**, 282 (2006).